The Dynamics of Vortex Rossby Waves and Secondary Eyewall Development in Hurricane Matthew (2016): New Insights from Radar Measurements

STEPHEN R. GUIMOND

University of Maryland, Baltimore County, Baltimore, and NASA Goddard Space Flight Center, Greenbelt, Maryland

PAUL D. REASOR

NOAA/Hurricane Research Division, Miami, Florida

GERALD M. HEYMSFIELD AND MATTHEW M. MCLINDEN

NASA Goddard Space Flight Center, Greenbelt, Maryland

(Manuscript received 12 October 2019, in final form 29 April 2020)

Introduction

- A wave phenomenon may govern the structure of eyewall and rainband of hurricane. Early studies postulated that spiral bands were initiated by inertia-buoyancy waves. Inner-core bands are produced from breaking of vortex Rossby waves (VRWs) and propagate along PV gradient. (Kurihara 1976; Willoughby 1978; Guinn and Schubert 1993)

- There is a ring of enhanced vorticity in a TC at mature stage. The structure supports counterpropagating VRWs that can grow and lead to breakdown the eyewall into coherent turbulent structures and propagate outward. (Schubert et al. 1999)

Introduction

- Spiral VRWs can propagate radially outward and increase their radial wavenumber due to the differential rotation of the vortex. The VRWs stagnate at a specific radius, interact with the mean flow, and lead to spin up (spin down) inward (outward) the radius. If VRWs can sustain the forcing for a long time, they modify the mean vortex structure. (Montgomery and Kallenbach 1997; Moller and Montgomery 2000)

- In model studies, VRWs can axisymmetrize the small-scale vorticity anomalies in outer regions of the vortex core by radially expanding large-scale vorticity and cause a secondary peak in tangential wind. (Kuo et al. 2008; Terwey and Montgomery 2008; Qiu et al. 2010)

Introduction

- Identifying VRW bands: The banded vorticity features have radial wavelengths of 6~10 km and are coupled to the convective filed. The azimuthal phase speed is consistent with the VRW theory. (Corbosiero et al. 2006; Didlake and Houze 2011)

- Theoretical estimates of VRW stagnation radii coincide with the region of secondary eyewall formation. (Fischer et al. 2020)

- Understanding the structure of spiral bands and the impact of secondary eyewall formations by Absolute angular momentum (AAM) equation by using highly temporal and spatial resolution measurement.

Data and processing

- Airborne Doppler radar:
  - The High-Altitude Imaging Wind and Rain Airborne Profiler (HIWRAP)
  - Conically and downwardly scanning
  - 16 rpm
  - 30^{o} and 40^{o} tilt angles (20 km and 30 km coverage)

- Aircraft:
  - NASA Global Hawk (GH) unmanned aircraft
  - 18-19 km height
  - Airspeed 160 m/s

Data and processing

- Wind:
  - Three-dimensional variational algorithm (3DVAR)
  - No Laplacian filter
  - Two-point running-mean filter
  - 1-km horizontal and 0.25-km vertical spacing
  - Wind vector is storm-relative.

- Reflectivity:
  - HIWRAP
  - WSR-88D located at Melbourne , Jacksonville, Florida
    - 1-km horizontal and 1^o azimuthal spacing

- Storm center:
  - Air Force and NOAA aircraft
  - 4.61 m/s (16.6 km/hr) toward north-northeast

Overview of Hurricane Matthew

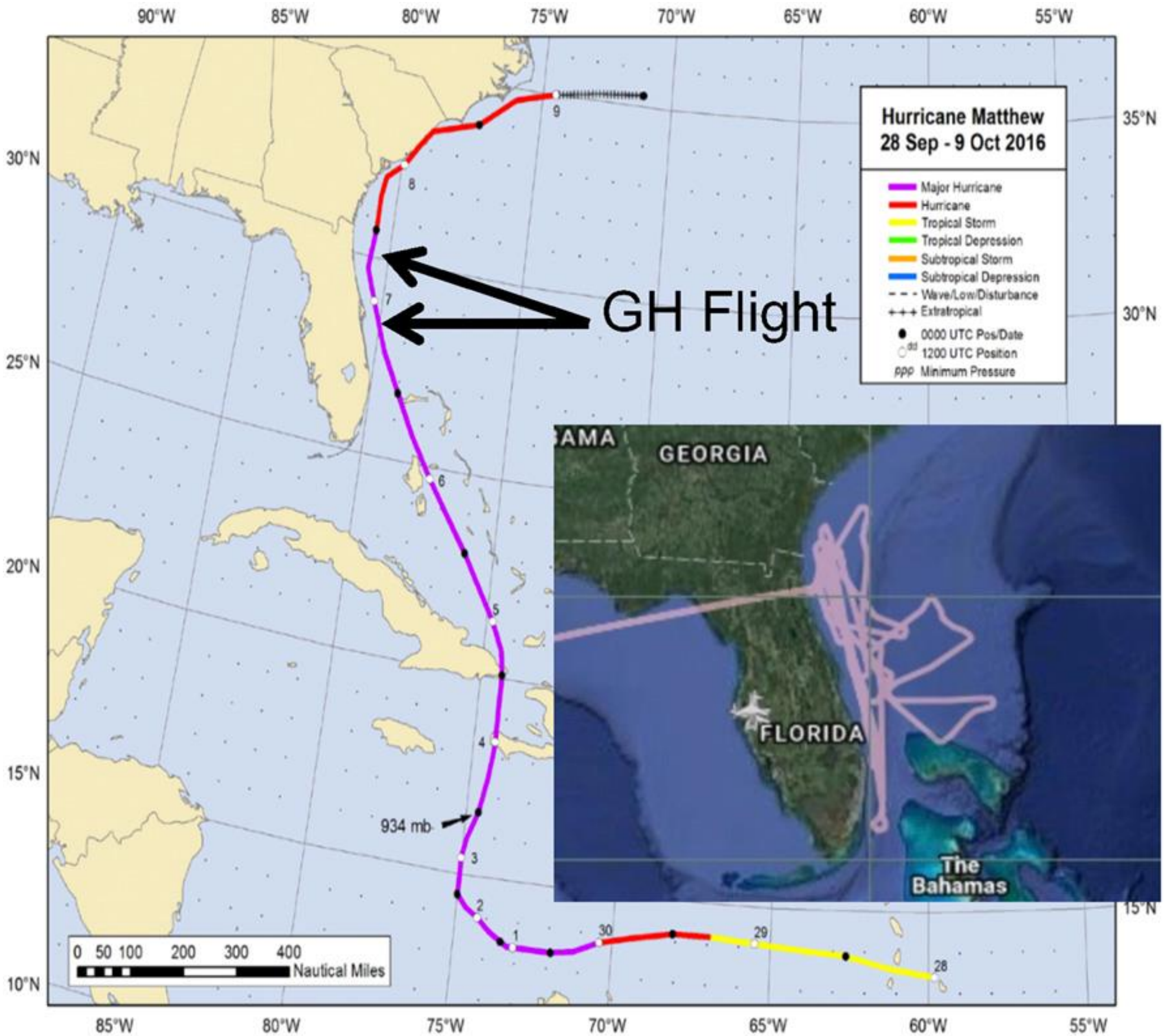

Best track (NHC)

GT aircraft during 10/7 10~20 Z

Overview of Hurricane Matthew

Intensity (NHC)

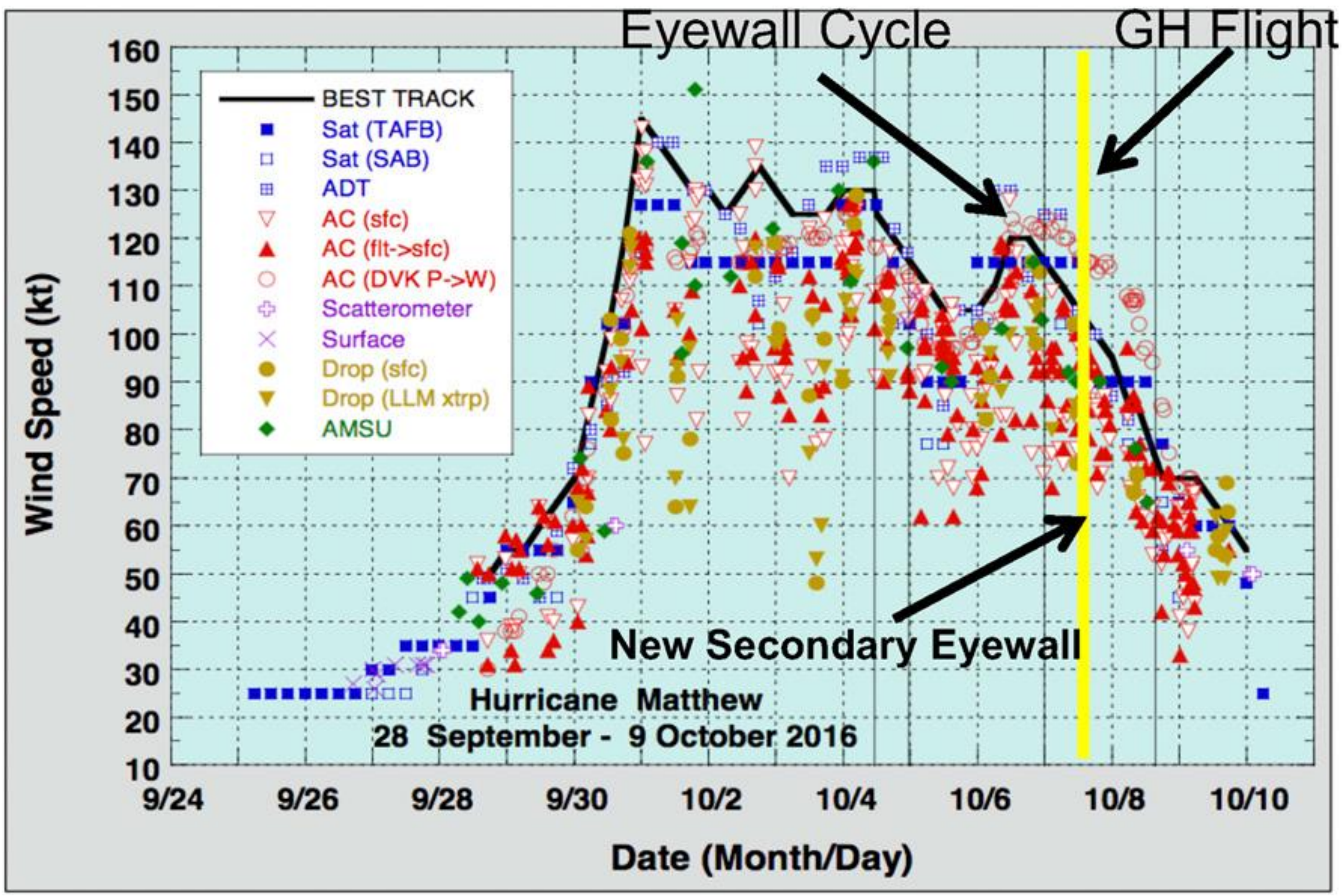

RI: 75 kt in 24 hr

Shear: 9 m/s, southwesterly

VRW Remote Sensing Observations

Melbourne Radar (dBZ)

1047

1155

White arrow: shear vector

Thin dashed line: Distance from radar per 50 km

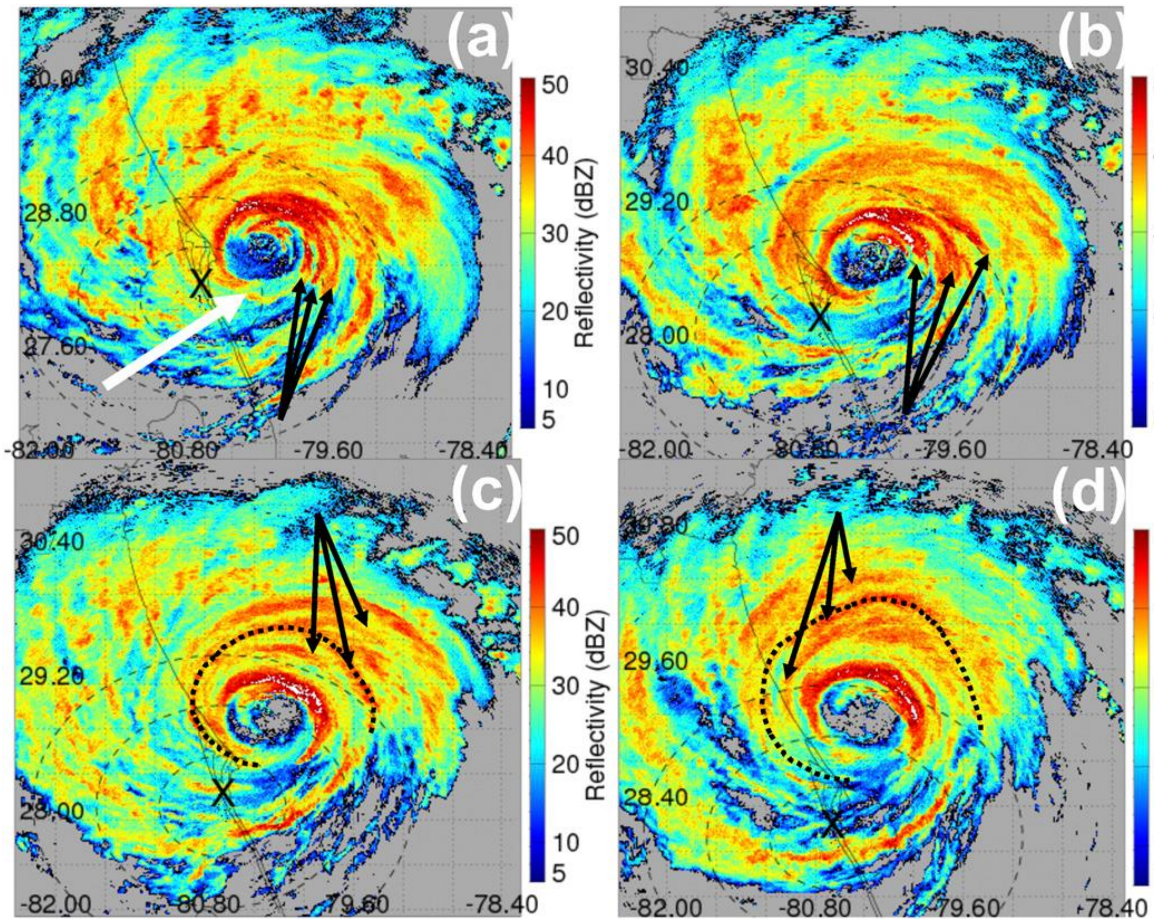

1240

1348

VRW Remote Sensing Observations

Two overpasses composite

Average between 1~1.5 km height (1811 and 1900)

Gray arrow: shear vector

dBZ (HIWRAP)
Perturbation wind

Dotted line: The band structure

Vorticity

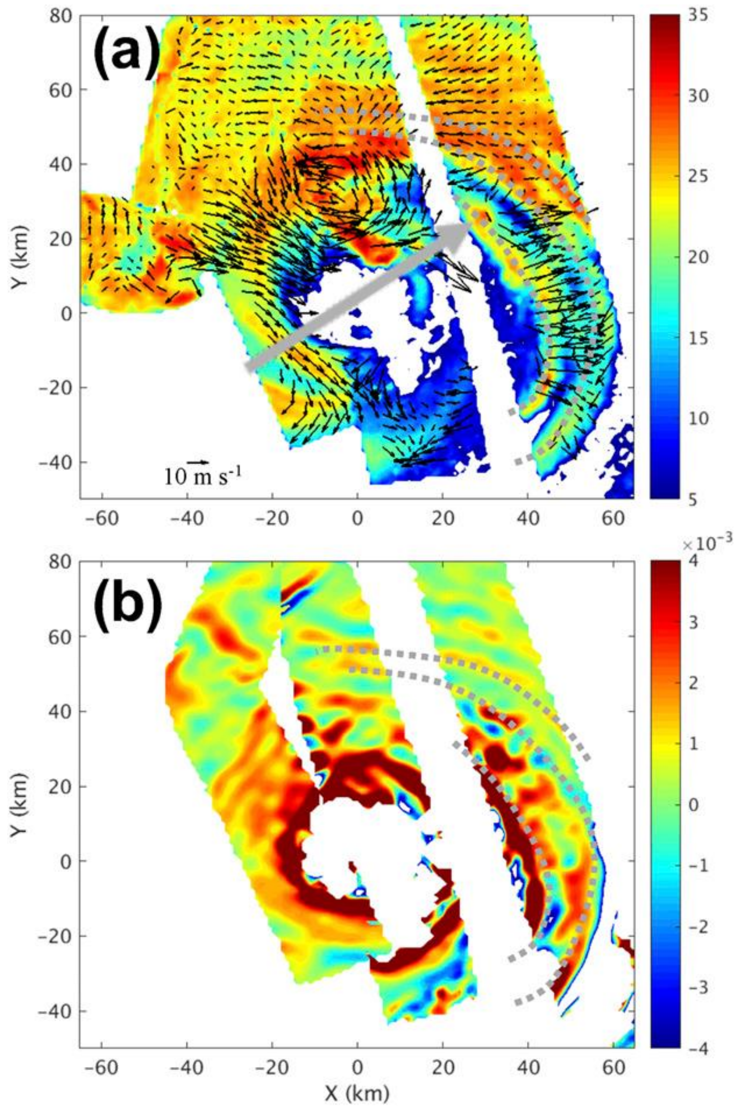

VRW Remote Sensing Observations

dBZ (WSR-88D) | dBZ (WSR-88D) | dBZ (wavenumber 2)

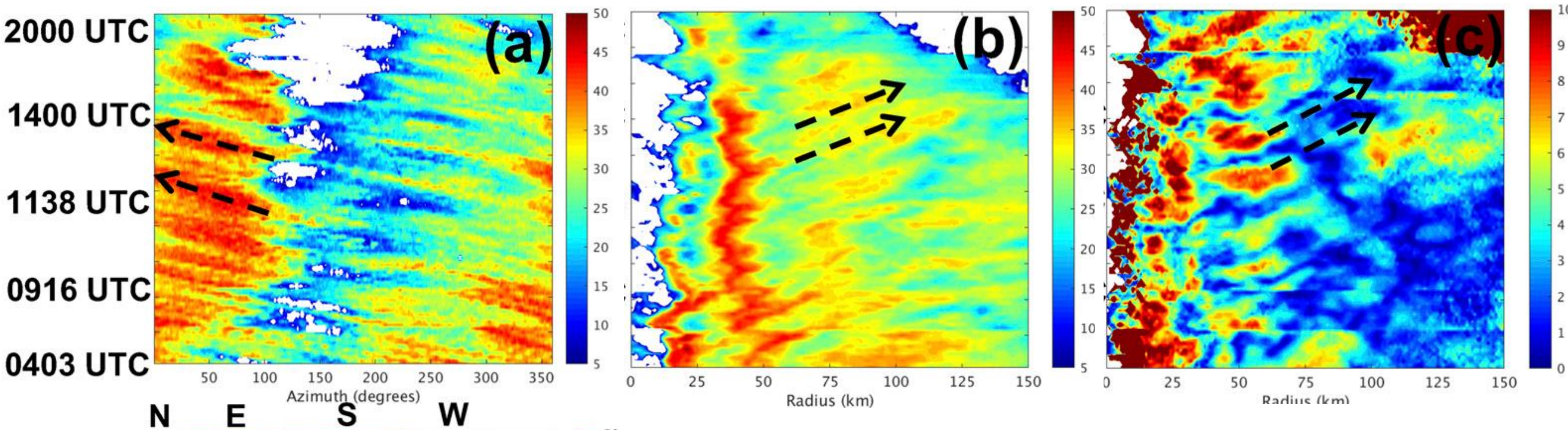

Azimuth | Radius | Radius

50-km radius | Avg over 10^o Northwest | Avg over 10^o Northwest

Azimuthal phase speed = Advection by earth-relative flow + Intrinsic propagation speed

24.5 m/s | 39 m/s | -14.5 m/s

Intrinsic propagation speed of WN1 derived by barotropic dispersion relation: -14.3 m/s
(Montgomery and Kallenbach, 1997)

VRW bands!

VRW Observations

1306~1345 overpass
2-km height wind
1326 WSR-88D dBZ

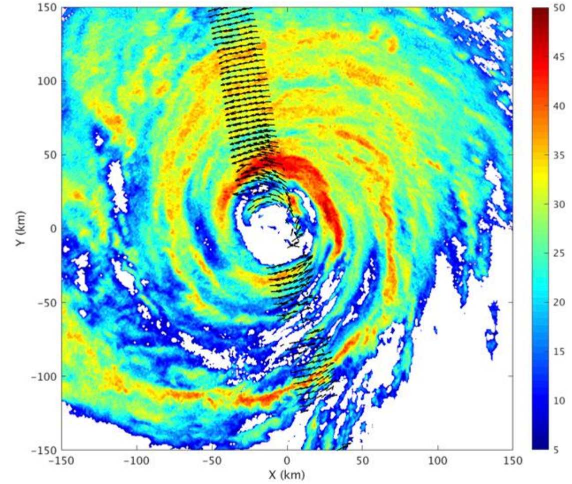

HIWRAP 2-km height

dBZ　　u　　w　　vorticity

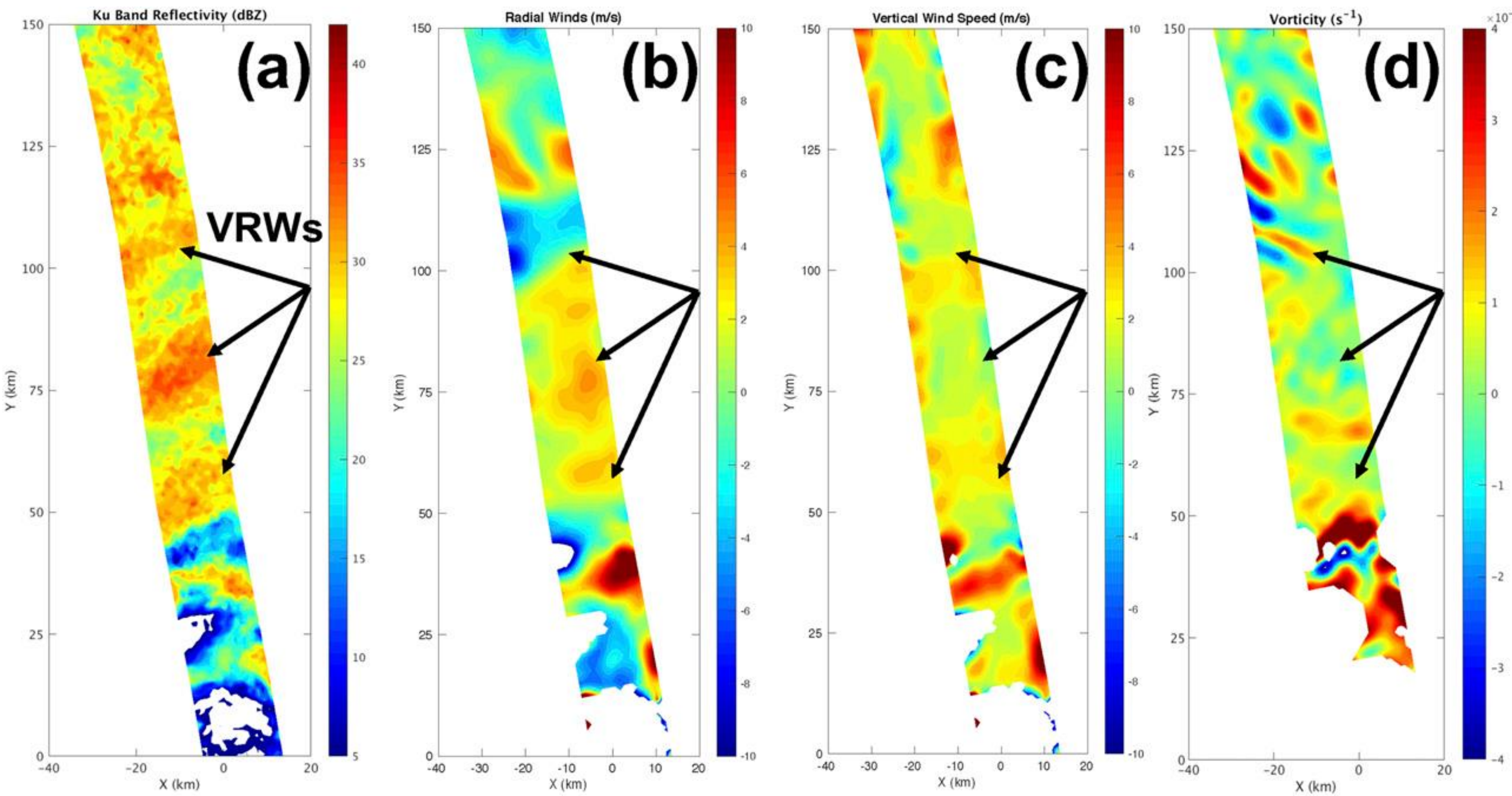

HIWRAP cross section

dBZ

u

w

v

vorticity

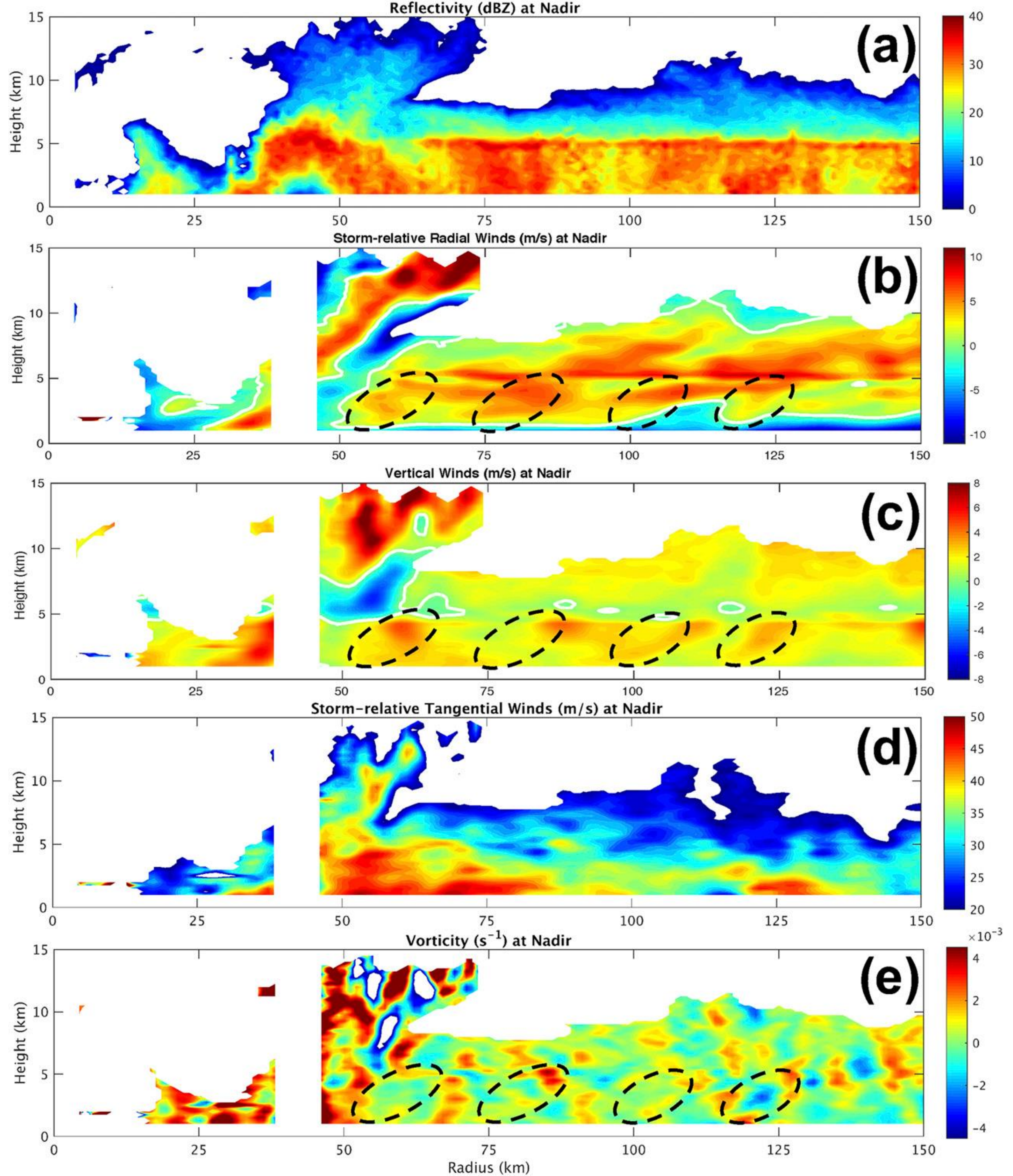

VRW Observations

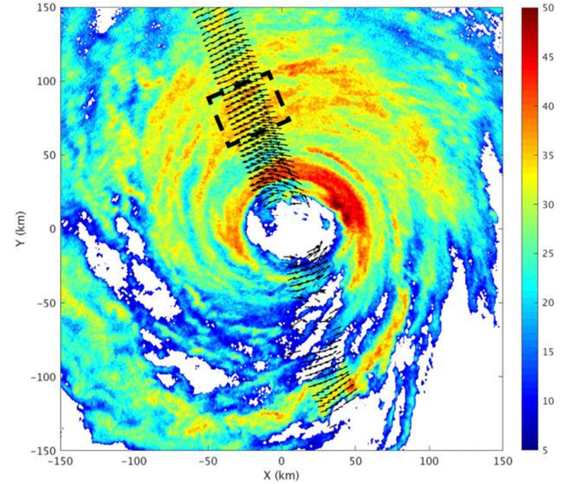

1345~1424 overpass
2-km height wind
1400 WSR-88D dBZ

HIWRAP 2-km height

u w v vorticity

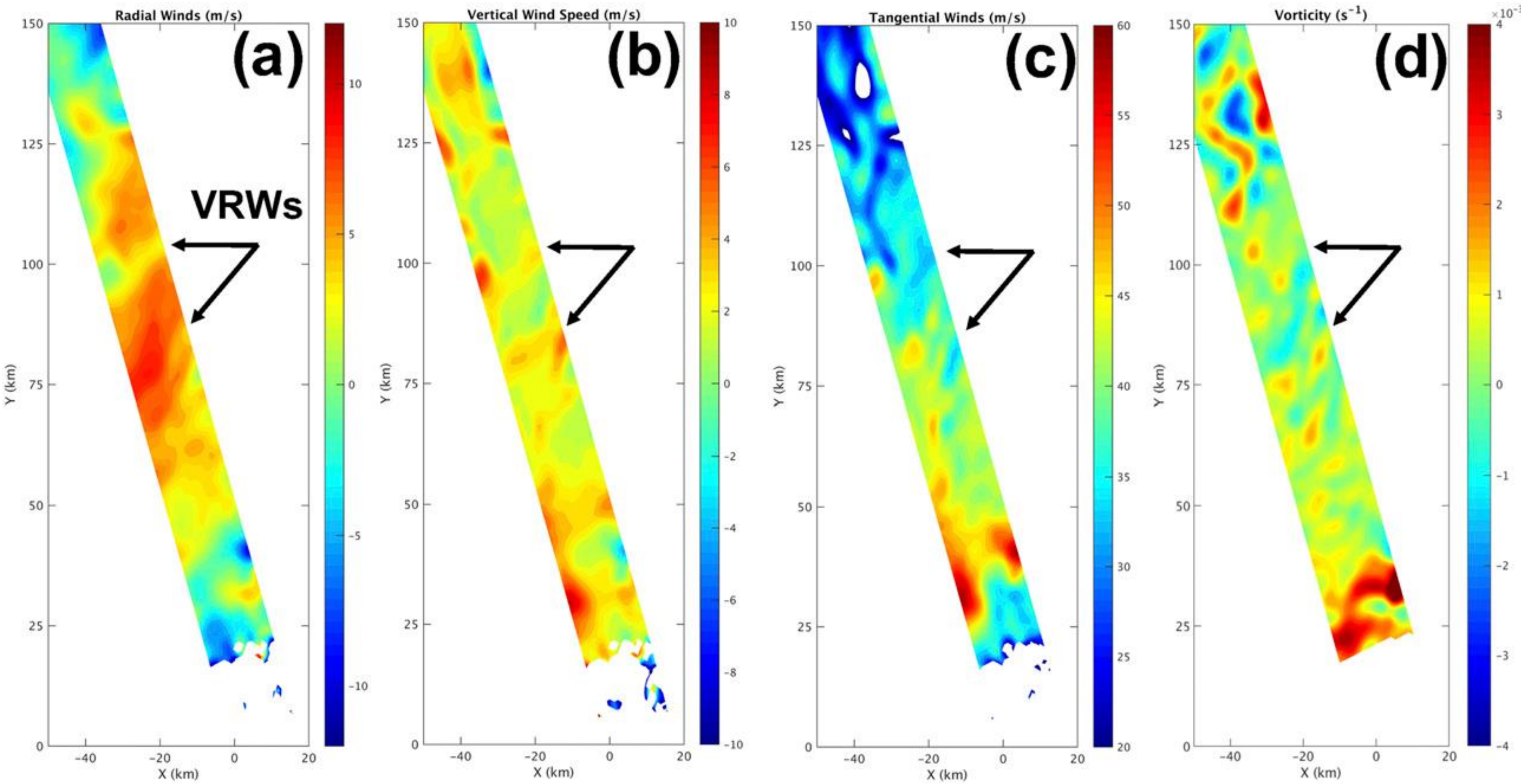

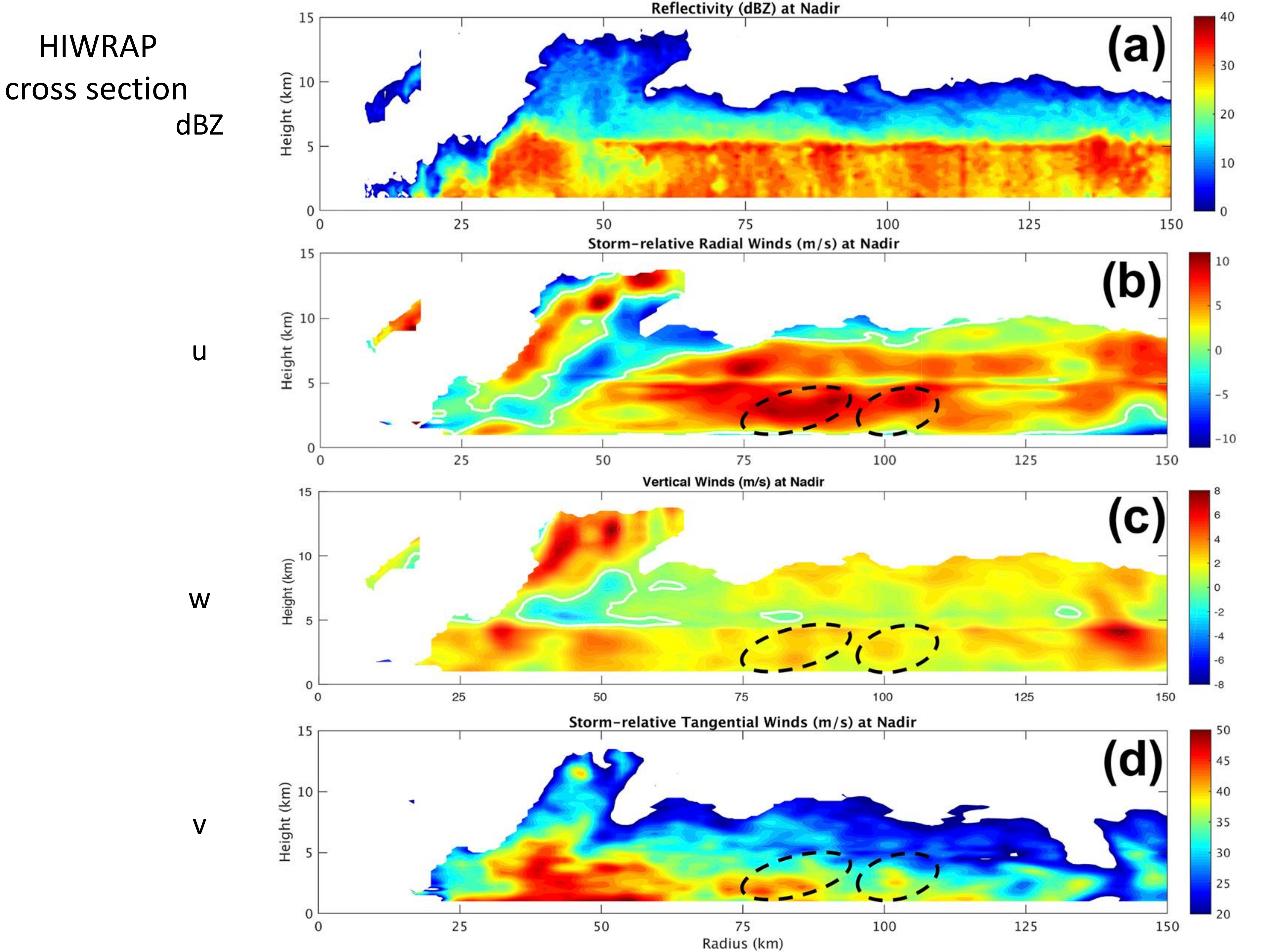

HIWRAP
cross section
dBZ
u
w
v
Reflectivity (dBZ) at Nadir
(a)
Storm-relative Radial Winds (m/s) at Nadir
(b)
Vertical Winds (m/s) at Nadir
(c)
Storm-relative Tangential Winds (m/s) at Nadir
(d)
Height (km)
Radius (km)

AAM Budget Analysis

Scale separation:

$$\tilde{\phi}(r,\theta,z) = \int \phi(r^*,\theta,z)G(r-r^*)dr^*$$

↑ top-hat filter

$$\phi'(r,\theta,z) = \phi(r,\theta,z) - \tilde{\phi}(r,\theta,z)$$

$\tilde{\phi}$: large scale

ϕ’: small scale

AAM Equation:

$$\frac{\partial \widetilde{M_a}}{\partial t} + \frac{1}{r}\frac{\partial r\tilde{u}\widetilde{M_a}}{\partial r} + \frac{1}{r}\frac{\partial \tilde{v}\widetilde{M_a}}{\partial \theta} + \frac{1}{\rho_0}\frac{\partial \rho_0 \tilde{w}\widetilde{M_a}}{\partial z} = -f_o r\widetilde{u_e} - \frac{1}{\rho_0}\frac{\partial \tilde{p}}{\partial \theta} - rSFS + rSGS$$

$$\widetilde{M_a} = r\tilde{v} + f_0\left(\frac{r^2}{2}\right)$$

$$\rho_0 = \rho_0(\mathrm{z})$$

SFS: sub-filter scale (2~15 km)

SGS: sub-grid scale (<2 km)

AAM Budget Analysis

20~30 km width

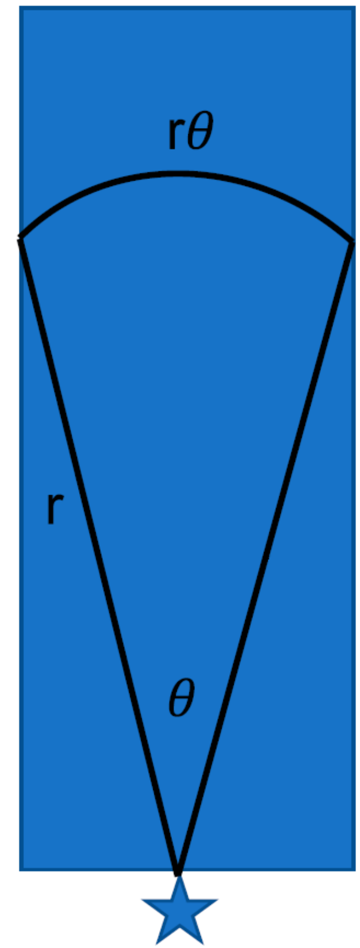

TC center

r = 130 km

Azimuthal Averaged AAM Equation:

$$\frac{\partial \overline{\widetilde{M}_a}}{\partial t} \cong -\frac{1}{r}\frac{\partial r\bar{\tilde{u}}\,\overline{\widetilde{M}_a}}{\partial r} - \frac{1}{\rho_0}\frac{\partial \rho_0 \bar{\tilde{w}}\overline{\widetilde{M}_a}}{\partial z} - r\overline{SFS} + r\overline{SGS}$$

$$\overline{SGS} = \frac{1}{r^2}\frac{\partial r^2\left(\overline{K_r}\frac{\partial \bar{\tilde{v}}}{\partial r}\right)}{\partial r} + \frac{1}{\rho_0}\frac{\partial \rho_0\left(\overline{K_z}\frac{\partial \bar{\tilde{v}}}{\partial z}\right)}{\partial z}$$

(Stull 1988)

$$\overline{K_r} = (C_s\Delta)^2\sqrt{2\left(\frac{1}{2}\frac{\partial \bar{\tilde{v}}}{\partial r}\right)^2} \qquad \Delta = 1000\ m$$

$$\overline{K_z} = (C_s\Delta)^2\sqrt{2\left(\frac{1}{2}\frac{\partial \bar{\tilde{v}}}{\partial z}\right)^2} \qquad \Delta = 250\ m$$

(Smagorinsky 1963)

$$\phi(r,z) = \frac{1}{r\theta}\int_0^{r\theta}\phi(r,\theta,z)\,r\,d\theta^*$$

AAM Budget Analysis

20~30 km width

Azimuthal Averaged AAM Equation:

$$\frac{\partial \overline{\widetilde{M_a}}}{\partial t} \cong -\frac{1}{r}\frac{\partial r\bar{\tilde{u}}\,\overline{\widetilde{M_a}}}{\partial r} - \frac{1}{\rho_0}\frac{\partial \rho_0 \bar{\tilde{w}}\overline{\widetilde{M_a}}}{\partial z} - r\overline{SFS} + r\overline{SGS}$$

$$\overline{SFS} = \frac{1}{r^2}\frac{\partial r^2\overline{\tau_{r\theta}}}{\partial r} + \frac{1}{\rho_0}\frac{\partial \rho_0\overline{\tau_{z\theta}}}{\partial z}$$

$$\overline{SFS} = \frac{1}{r^2}\frac{\partial r^2\overline{\tau_{r\theta}}}{\partial r} + \frac{1}{\rho_0}\frac{\partial \rho_0\overline{\tau_{z\theta}}}{\partial z}$$

$$\tau_{r\theta} = \left(\widetilde{\tilde{u}\tilde{v}} - \tilde{\tilde{u}}\tilde{\tilde{v}}\right) + \left(\widetilde{\tilde{u}v'} + \widetilde{u'\tilde{v}} - \tilde{\tilde{u}}\widetilde{v'} - \tilde{\tilde{v}}\widetilde{u'}\right) + \left(\widetilde{u'v'} - \widetilde{u'}\widetilde{v'}\right)$$

$$\tau_{z\theta} = \left(\widetilde{\tilde{w}\tilde{v}} - \tilde{\tilde{w}}\tilde{\tilde{v}}\right) + \left(\widetilde{\tilde{w}v'} + \widetilde{w'\tilde{v}} - \tilde{\tilde{w}}\widetilde{v'} - \tilde{\tilde{v}}\widetilde{w'}\right) + \left(\widetilde{w'v'} - \widetilde{w'}\widetilde{v'}\right)$$

Leonard stress | Cross stress | Reynolds stress

TC center

r = 130 km

$$\phi(r,z) = \frac{1}{r\theta}\int_0^{r\theta}\phi(r,\theta,z)\,rd\theta^*$$

Analysis for 1306-1345 Z

(large scale)

AAM

v

u

w

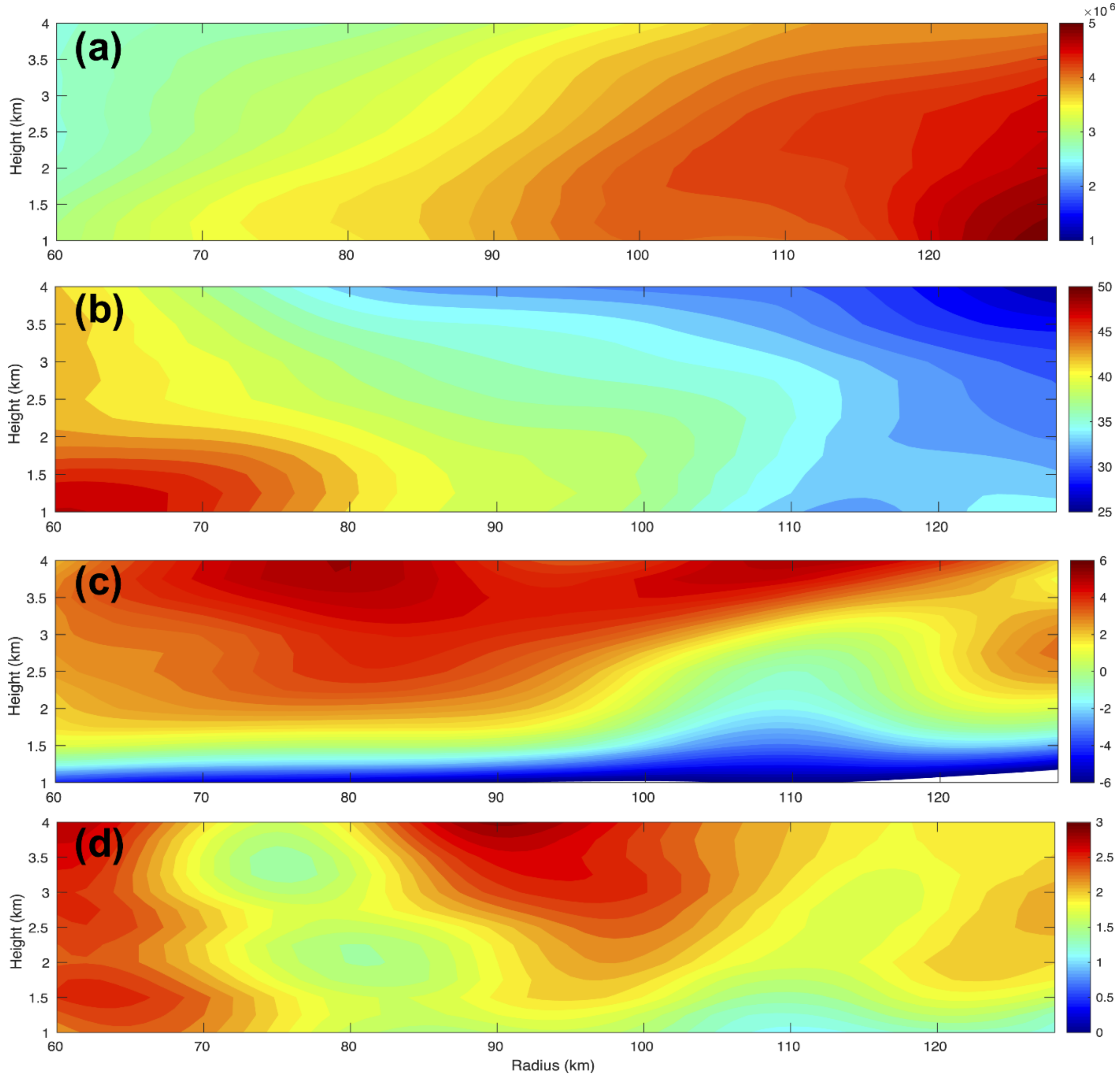

Analysis for 1306-1345 Z

(small scale) vorticity

dBZ

u

w

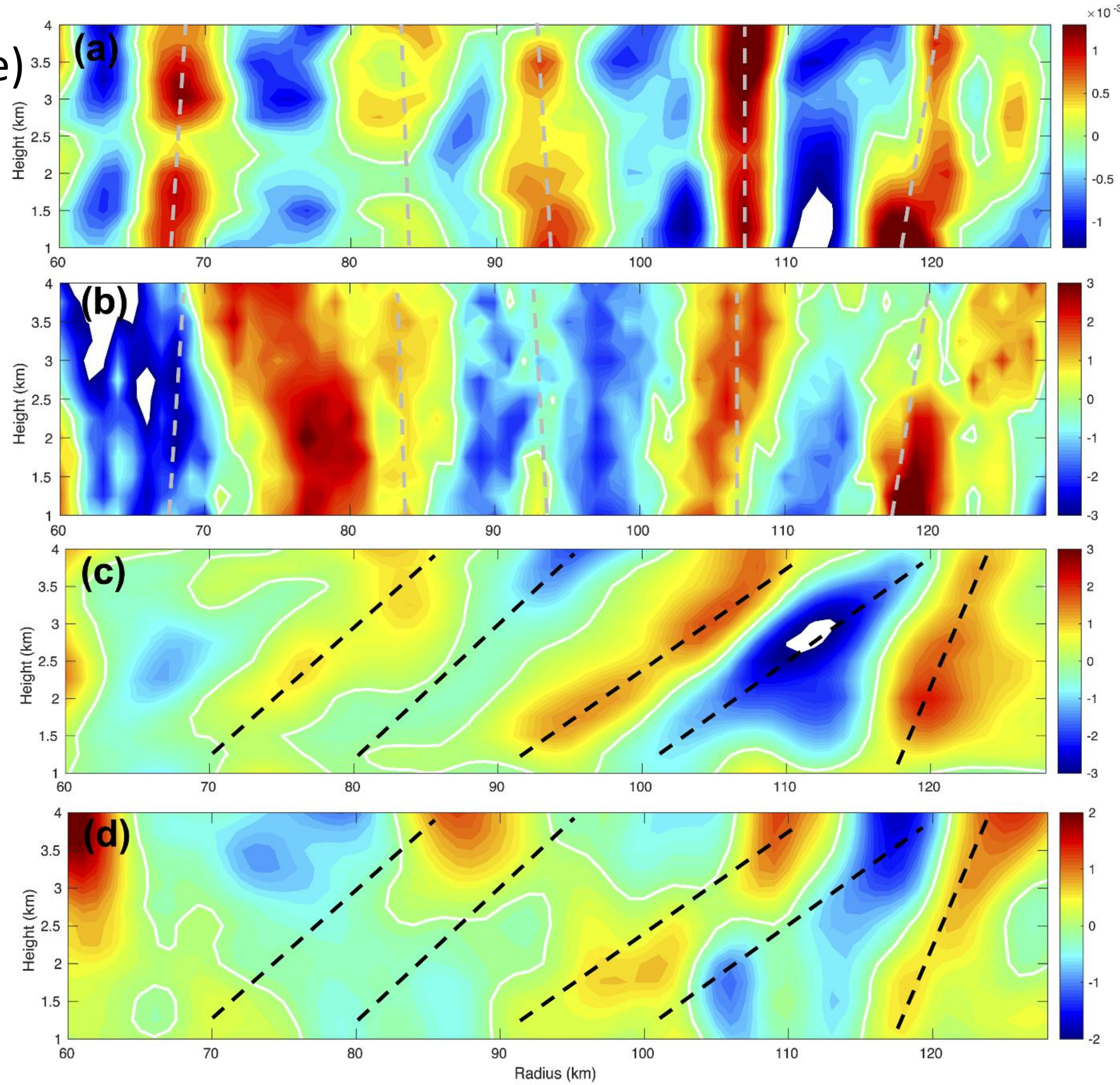

Phase line are the same.

Phase line are the same.

1306-1345 Z

$$\frac{\partial \overline{\widetilde{M}_a}}{\partial t}$$

$$-\frac{1}{\rho_0}\frac{\partial \rho_0 \bar{\tilde{w}}\overline{\widetilde{M}_a}}{\partial z}$$

$$-\frac{1}{r}\frac{\partial r\bar{\tilde{u}}\,\overline{\widetilde{M}_a}}{\partial r}$$

$$-r\overline{SFS}$$

$$\frac{1}{\rho_0}\frac{\partial \rho_0 \overline{\tau_{z\theta}}}{\partial z}$$

$$-r\overline{SFS}$$

$$\frac{1}{r^2}\frac{\partial r^2 \overline{\tau_{r\theta}}}{\partial r}$$

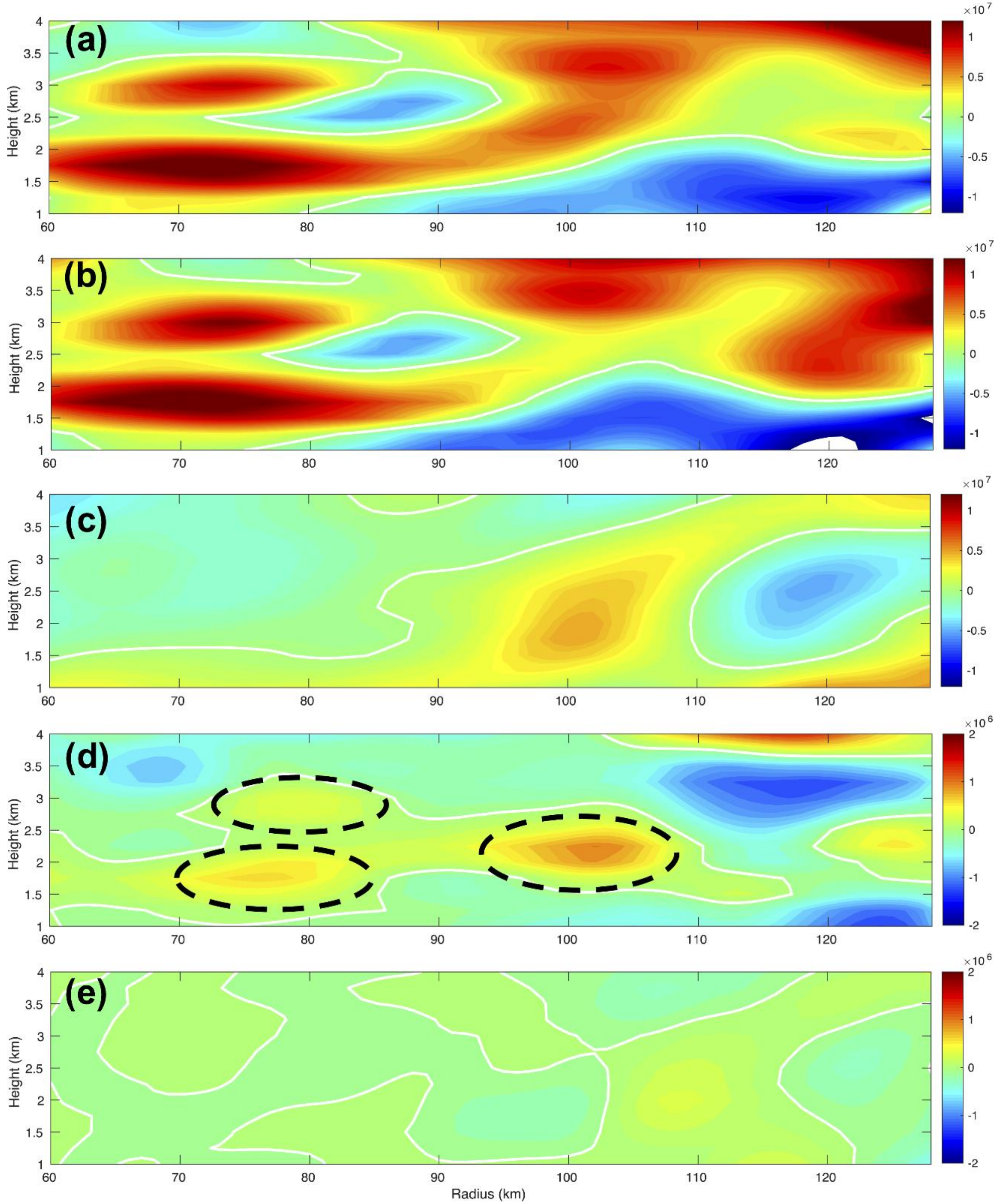

1306-1345 Z

$$-r\overline{SFS}$$

$$\frac{1}{\rho_0}\frac{\partial \rho_0 \overline{\tau_{z\theta}}}{\partial z}$$

Reynolds stress (small-small)

Cross stress (large-small)

Leonard stress (large-large)

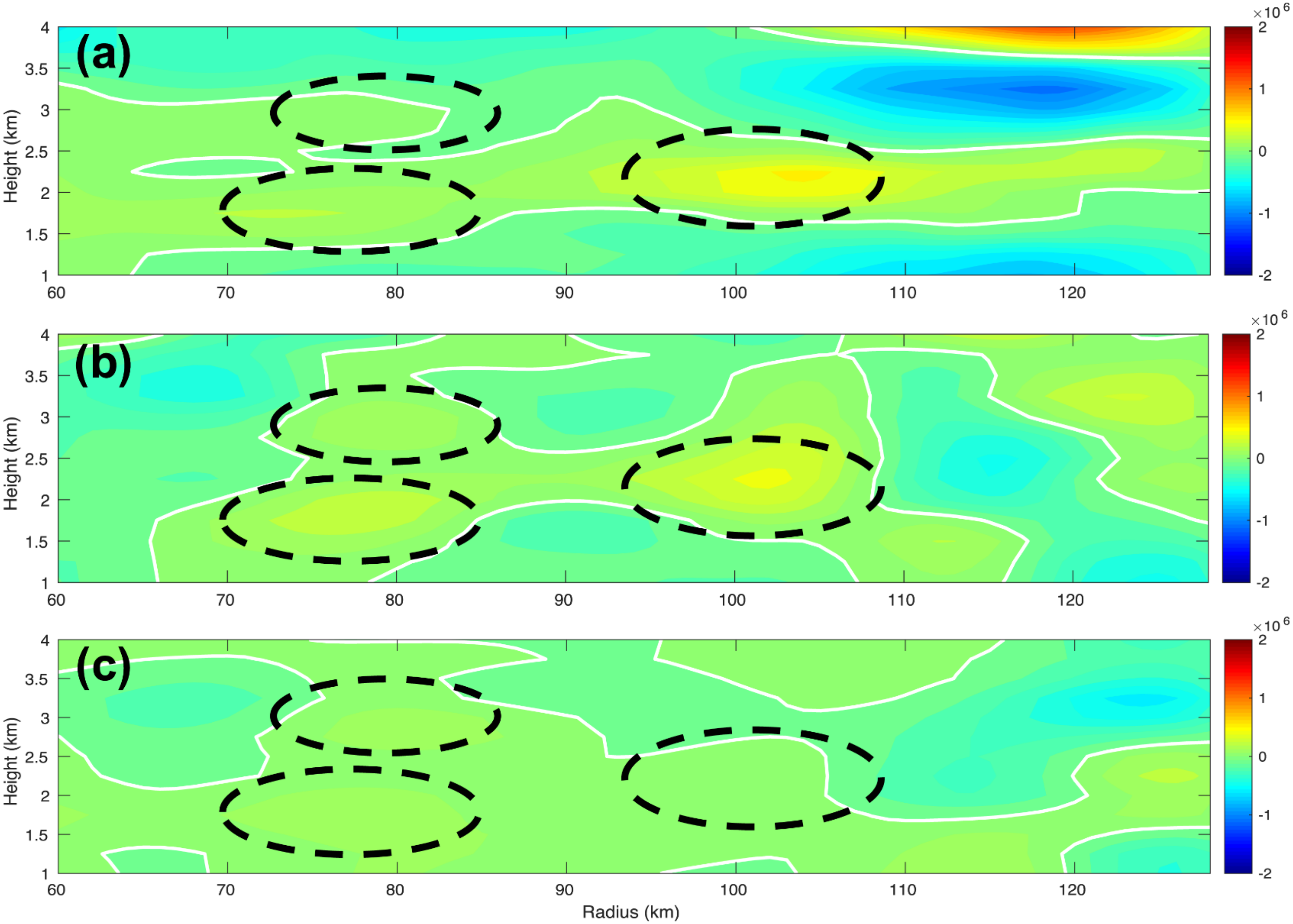

Physical Interpretation

AAM

v

w

$$-\frac{1}{\rho_0}\frac{\partial \rho_0 \overline{\widetilde{w}}\,\overline{\widetilde{M}_a}}{\partial z}$$

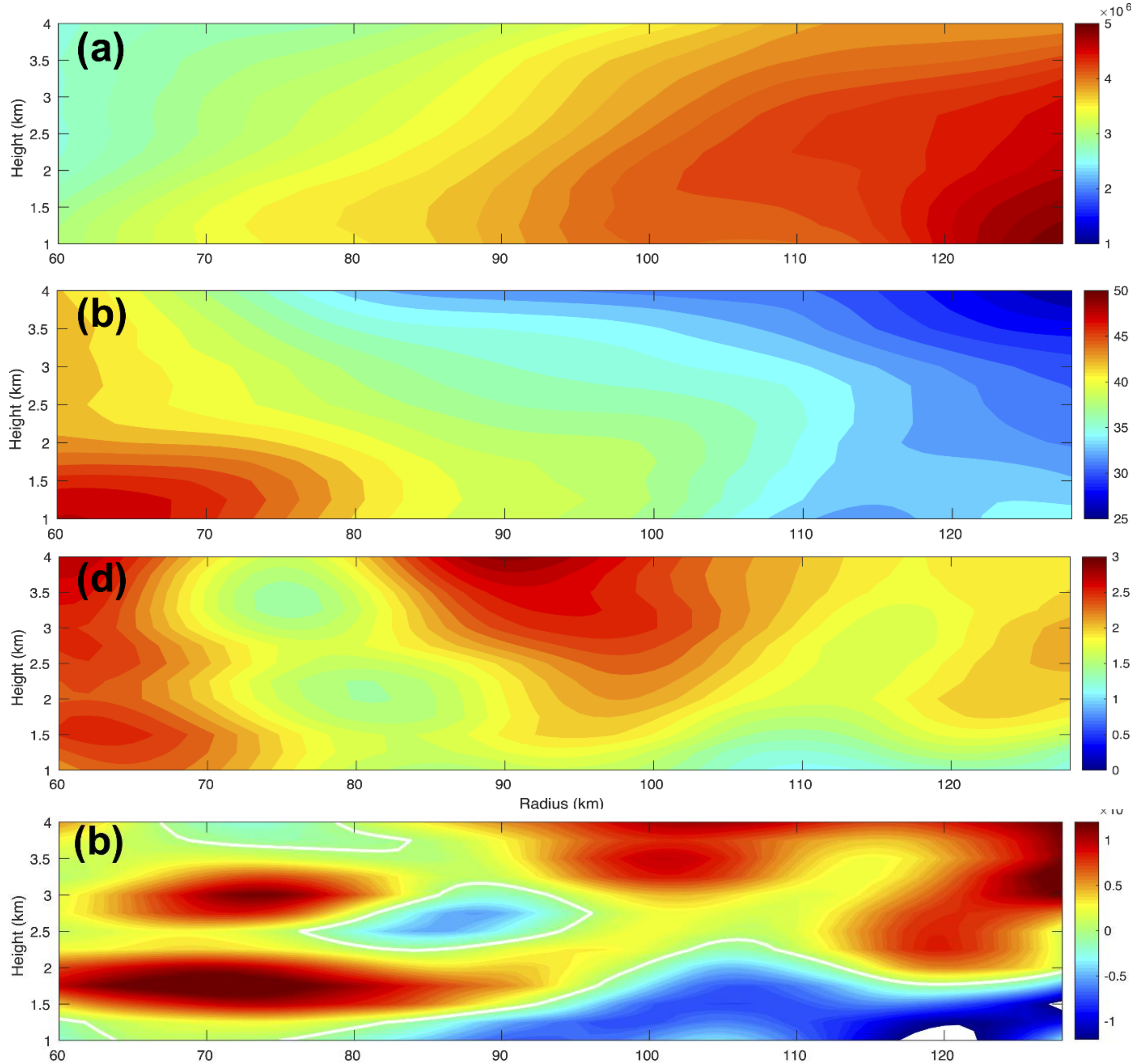

Physical Interpretation

AAM

u

$$-\frac{1}{r}\frac{\partial r\bar{\tilde{u}}\,\overline{\widetilde{M_a}}}{\partial r}$$

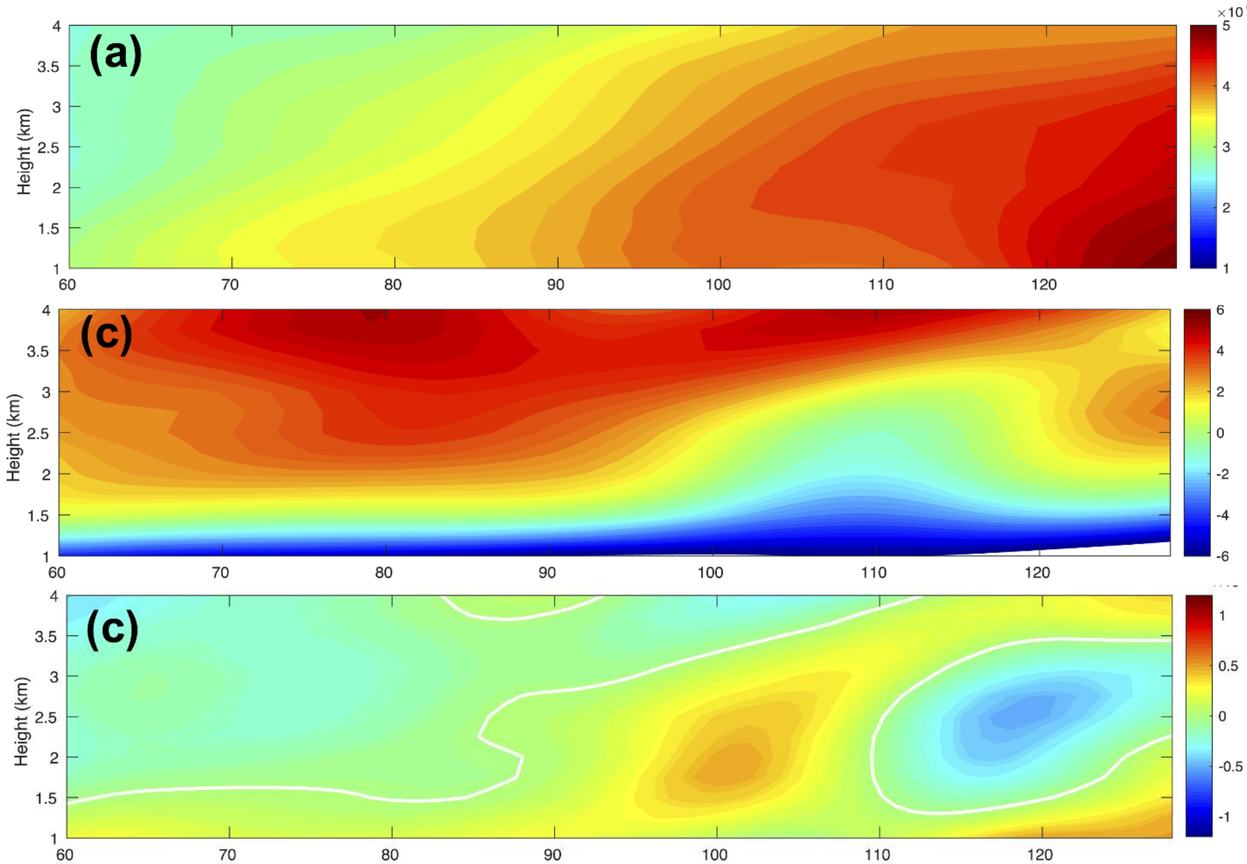

Physical Interpretation

$$\frac{\partial \overline{\widetilde{M}_a}}{\partial t}$$

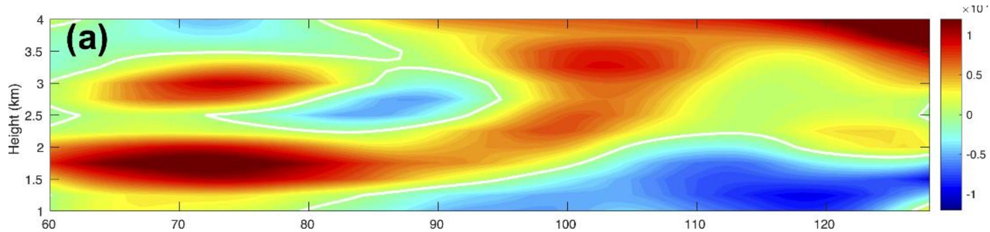

$$-\frac{1}{\rho_0}\frac{\partial \rho_0 \overline{\overline{w}}\,\overline{\widetilde{M}_a}}{\partial z}$$

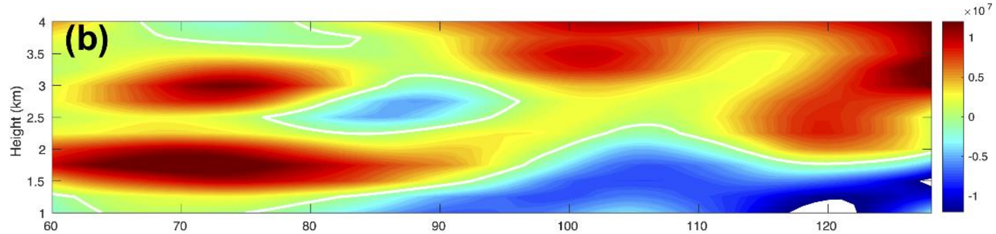

$$-r\overline{SFS}$$

$$\frac{1}{\rho_0}\frac{\partial \rho_0 \overline{\tau_{z\theta}}}{\partial z}$$

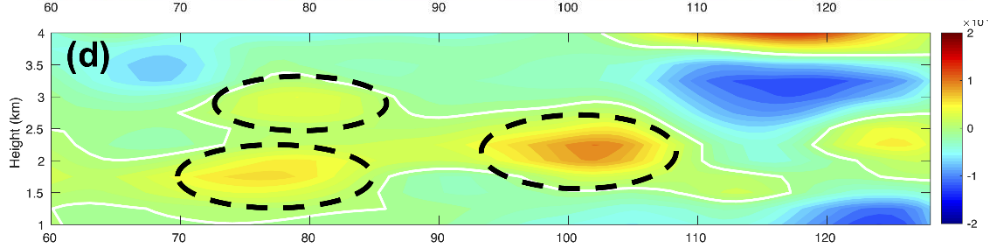

Forcing time scale: ~12 hr

Reynolds stress (small-small)

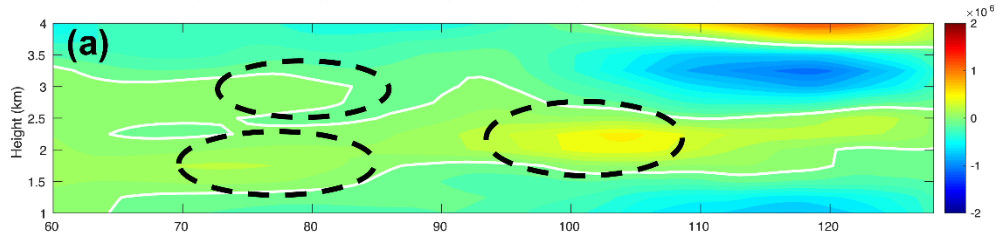

Cross stress (large-small)

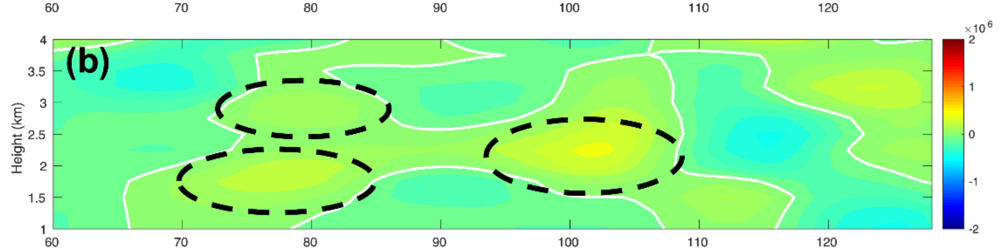

Physical Interpretation

Difference between 1306-1345 and 1345-1424

(large scale)

AAM

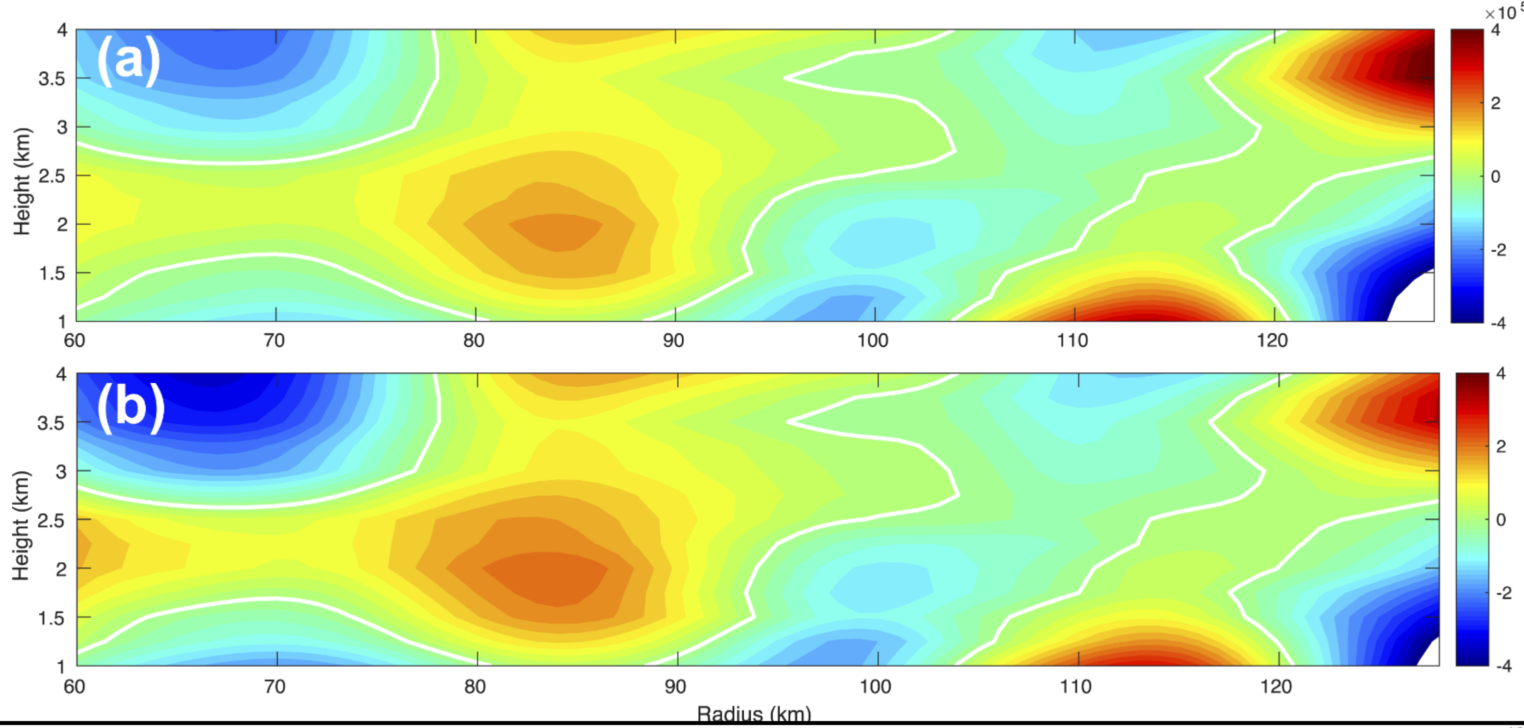

v

$$\frac{\partial \overline{\widetilde{M}_a}}{\partial t}$$

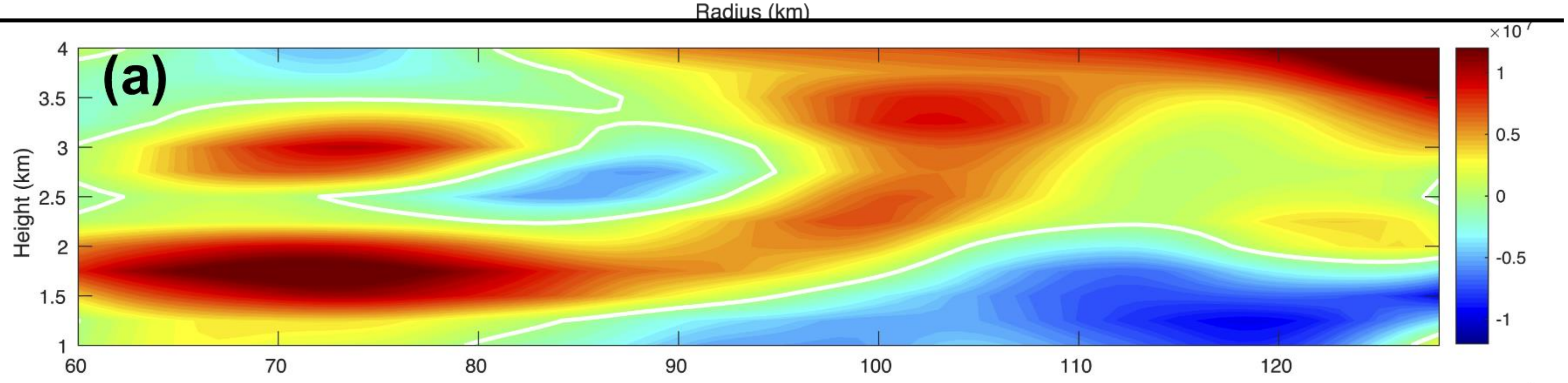

1345-1424 Z

$$\frac{\partial \overline{\widetilde{M_a}}}{\partial t}$$

$$-\frac{1}{\rho_0}\frac{\partial \rho_0 \overline{\widetilde{w}}\overline{\widetilde{M_a}}}{\partial z}$$

$$-\frac{1}{r}\frac{\partial r \bar{\widetilde{u}}\ \overline{\widetilde{M_a}}}{\partial r}$$

$$-r\overline{SFS}$$

$$\frac{1}{\rho_0}\frac{\partial \rho_0 \overline{\tau_{z\theta}}}{\partial z}$$

$$-r\overline{SFS}$$

$$\frac{1}{r^2}\frac{\partial r^2 \overline{\tau_{r\theta}}}{\partial r}$$

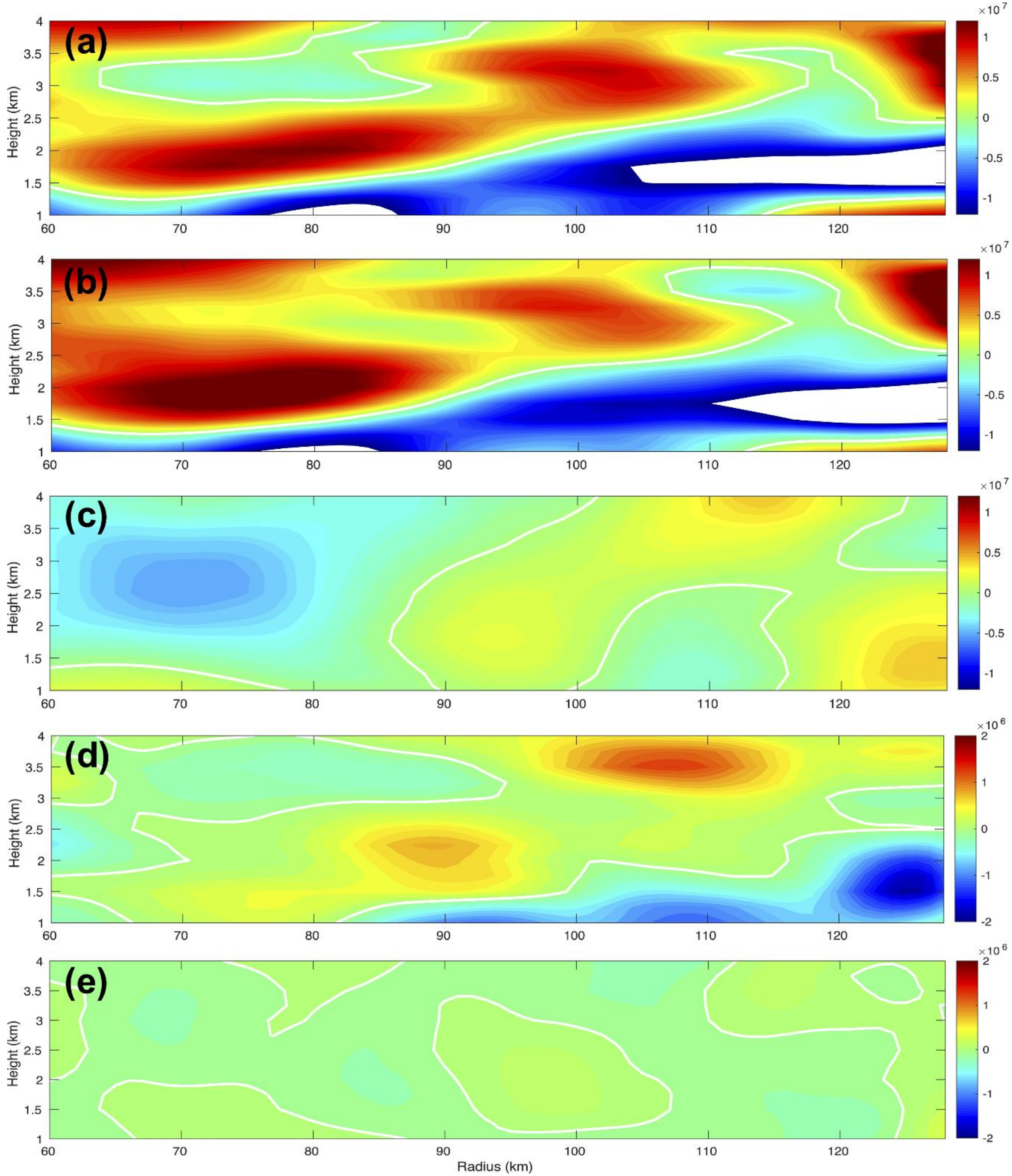

1345-1424 Z

$$-r\overline{SFS}$$

$$\frac{1}{\rho_0}\frac{\partial \rho_0 \overline{\tau_{z\theta}}}{\partial z}$$

Reynolds stress
(small-small)

Cross stress
(large-small)

Leonard stress
(large-large)

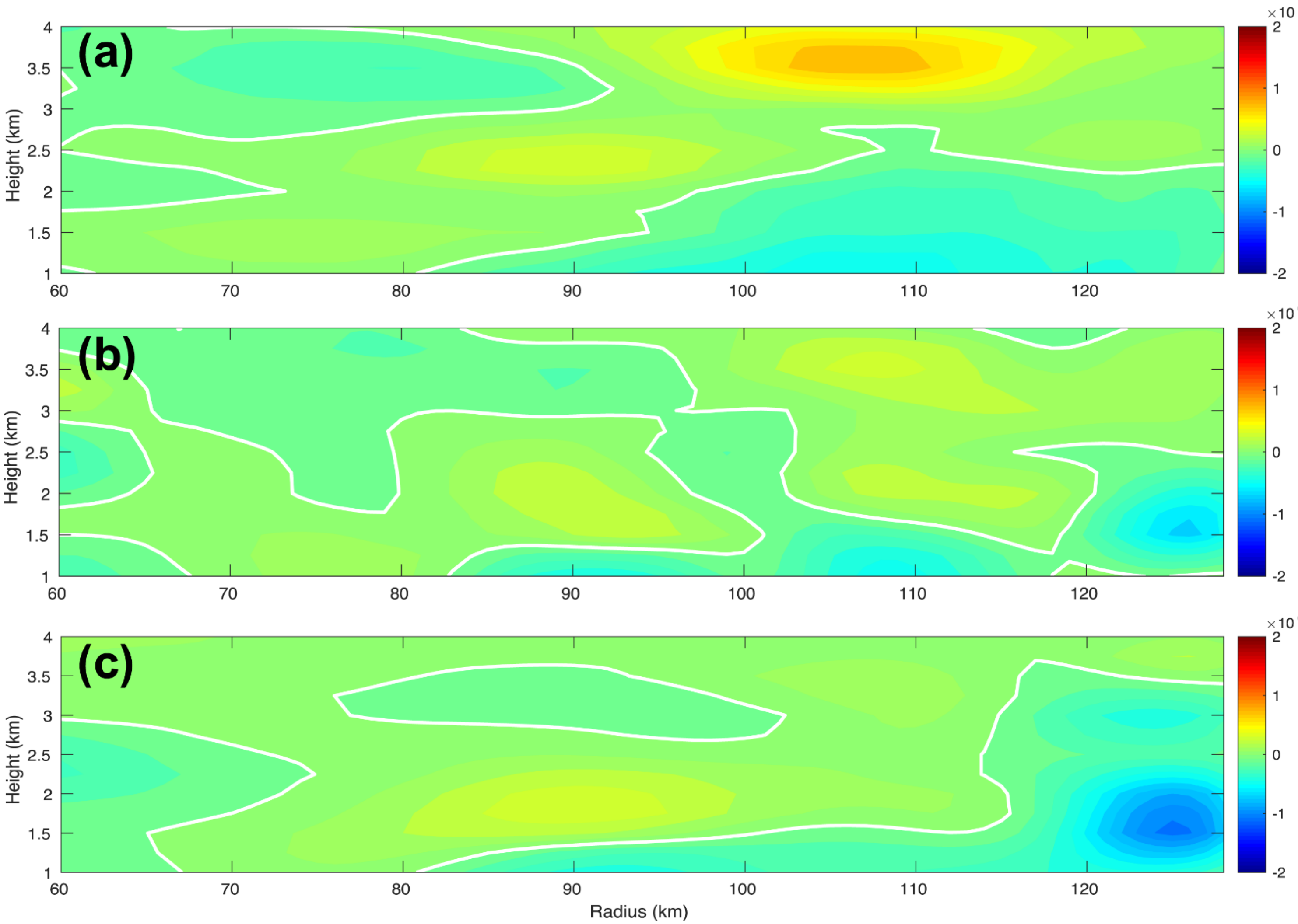

Air Force aircraft observation

3-km height

Aircraft tracks

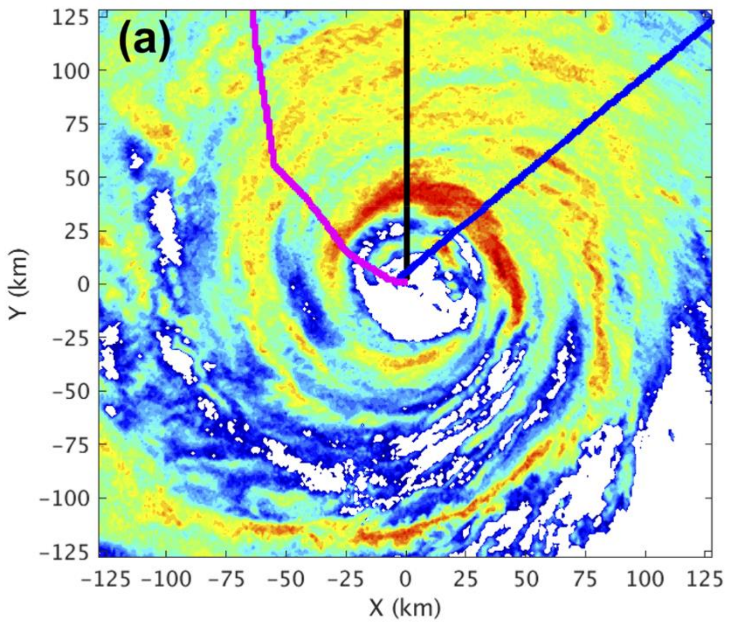

Color: 1325 Z dBZ (WSR-88D)

v

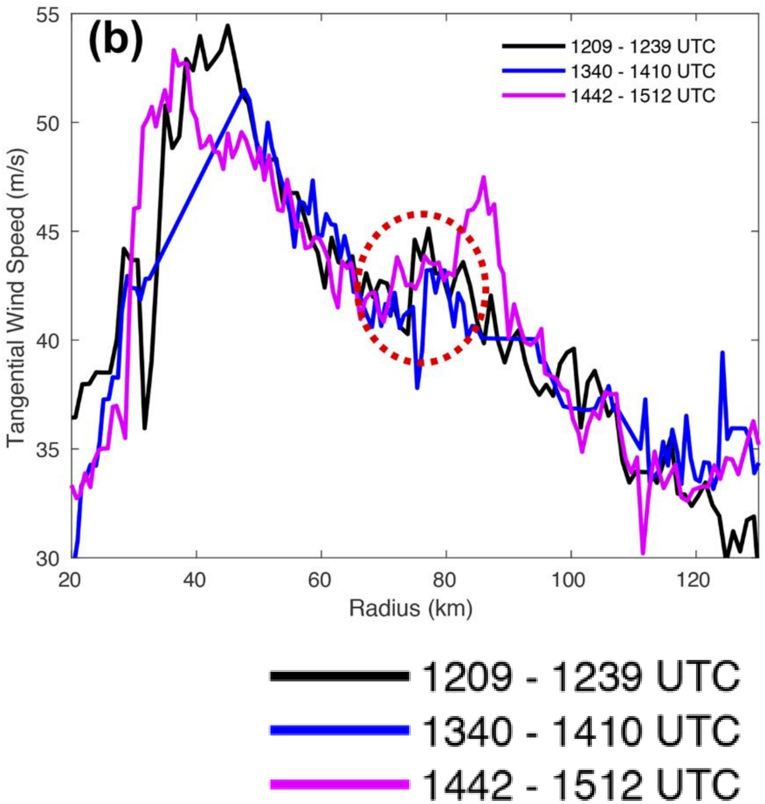

Summary

- The eyewall of Hurricane Matthew (2016) broke into bands in the downshear-right quadrant of the storm and spread in radius and azimuth with radial wavelength 12~15 km.

- The azimuthal phase speeds of the bands were -14.5 m/s, which were consistent with barotropic VRW theory. Reflectivity, vorticity, radial wind, and vertical velocity had positive correlations were regarded as VRW bands, which were most active in the 75-125 km radial bands.

Summary

- In the AAM budget analysis, large-scale vertical flux convergence of AAM had the largest contribution to $\partial\overline{\widetilde{M_a}}/\partial t$. VRW act to lift and converge higher AAM found at low-levels. The secondary tangential wind maxima were observed in the 75-80 km radial region where $\partial\overline{\widetilde{M_a}}/\partial t$ were positive.

- The VRWs were transporting higher angular momentum from the inner-core region to the outer-core region where they meet inflow and lead to an acceleration.

- Reynolds stress and cross stress contributed forcing to large-scale AAM. If the forcing sustain for a long time, the effect can be integrated and can be projected on to wavenumber 0 or 1 by mean vortex flow to change the structure of TC.